Anderson Localization

Daniel Bruns, Rafael Haenel, and Gary Tom
(Dated: November 25, 2017)

Localization phenomena in disordered systems have attracted great theoretical interest since the second half of the 20th century. In this article we give an introduction to the theory of Anderson-localization. We perform numerical calculations of eigenstates of disordered tight-binding Hamiltonians in 1D and 3D and review recent experimental evidence of localization of bosonic wavefunctions in a 1D-magneto-optical trap. Additionally, we provide a brief overview of the effect of Hubbard electron-electron interactions and their implications on the Eigenstate Thermalization Hypothesis.

I. INTRODUCTION

In 1958, Philip Anderson published his seminal paper on how certain materials can undergo a phase transition from conductor to insulator when the amount of disorder in the system passes a certain threshold [1]. This sudden reduction in conduction is associated with the localization of the electronic wavefunction; when the state no longer is extended, and instead is spatially localized. In 1977, Anderson was awarded the Nobel Prize, in part for his work on localization phenomena.

Anderson localization, as it is now known, can be understood as an interference phenomenon. In the original tight-binding model formulated by Anderson, electrons are able to tunnel between neighbouring lattice sites. However, at high enough disorder in the lattice, the quantum amplitudes associated with tunnelling paths cancel each other, resulting in a localized wavefunction. An equivalent wave model has been proposed, in which the incoming wave is scattered off of potentials generated by the disorder. At a high enough disorder, the scattered wavelets interfere destructively in the forward direction, causing the wave to decay exponentially [2].

Since his original paper, advances in computing technologies have allowed for precise numerical studies of Anderson localization. Experimental efforts have largely confirmed Anderson localization in disordered materials, but direct observation of localized wavefunctions has only been done in 1D [3].

II. LOCALIZATION IN ONE DIMENSION

We consider the Anderson Hamiltonian [1], a tight-binding model with nearest-neighbor hopping and random on-site energy:

$$\hat{H} = W \sum_n \epsilon_n \hat{c}_n^\dagger \hat{c}_n + t \sum_{<n,m>} \left(\hat{c}_n^\dagger \hat{c}_m + \text{h.c.} \right). \qquad (1)$$

The on-site energy $\epsilon_n \in [-1/2, 1/2]$ is usually drawn from a uniform random distribution and W is the disorder parameter. In the future we set $t = 1$, thus effectively measuring all energies in units of t.

To draw some analytical conclusions, let us first consider a one dimensional chain of arbitrary length L with lattice spacing a. In the limit $W = 0$, the solutions are Bloch-states with energy dispersion $E(k) = 2t\cos(ka)$. If we have finite W, the eigenstates $|\Psi\rangle = \sum_n \psi(n)\hat{c}_n^\dagger |0\rangle$ are determined from the recursion relation

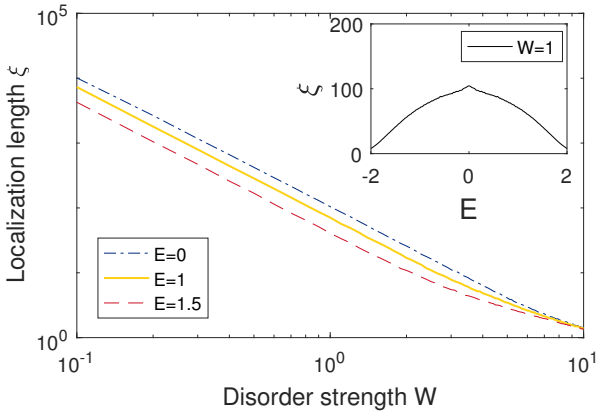

FIG. 1. Log-log scale plot of localization length ξ in 1D as a function of disorder W and energy E (inset). The data was numerically calculated by solving Eq. (2) with the transfer-matrix method. ξ is well fitted by $\xi = \alpha W^{-2.0}$ for all E and is smallest at the edge of the energy band.

$$E\psi(n) = \epsilon_n \psi(n) + \psi(n+1) + \psi(n-1). \qquad (2)$$

This may be rewritten using transfer-matrices T_i:

$$\begin{pmatrix} \psi(n+1) \\ \psi(n) \end{pmatrix} = \prod_{i=1}^{L} \hat{T}_i \begin{pmatrix} \psi(1) \\ \psi(0) \end{pmatrix}, \quad \hat{T}_i = \begin{pmatrix} E - \epsilon_i & -1 \\ 1 & 0 \end{pmatrix}.$$

By proving Fuerstenberg's theorem for products of random matrices, it can be rigorously shown that solutions $\psi(n)$ of Eq. (2) decay exponentially for $n \to \infty$ [4, 5], so that the overall shape of the wavefunction is $\psi(n) \sim \exp(-n/\xi)$. Here, ξ is the localization length in units of lattice constant a. As a consequence, eigenstates are not extended over real-space but are exponentially confined to certain areas of the lattice. We will refer to these states as localized. Remarkably, we note that any state in a one dimensional system will be localized. This implies that any 1D material will lose its diffusion or conduction capabilities if the system size is $L > \xi$.

We can also solve Eq. (2) numerically. For this, we apply 10^6 transfer matrices to an initial vector

$(\psi(1), \psi(0)) = (1, \exp(ik))$, where k is the momentum of a tightly bound electron with a given energy E. The resulting coefficients $\psi(n)$ are averaged from 100 calculations with different realizations of randomness. We then extract the localization length ξ by exponentially fitting the coefficients. The results are displayed in Fig. 1. The disorder dependence of the localization is well described by the power law $\xi \propto W^{-2.0}$. Moreover, states at the edges of the energy band localize fastest.

III. SCALING THEORY

To assess localization properties in higher dimensions, we will examine the effects of scaling on the conductance of a system. These scaling arguments were first presented by Abrahams, Anderson, Licciardello, and Ramakrishnan, after the concept of Renormalization Group was introduced [6].

Let us define the dimensionless conductance for a d-dimensional cube of size L^d

$$g(L) = \frac{T(L)}{1 - T(L)}, \tag{3}$$

where $T(L)$ is the transmission in one direction. Intuitively, T scales as $T(bL) = T(L)^b$. Considering that the cross-section perpendicular to the direction of transmission increases with $b^{(d-1)}$, we obtain an expression for the new conductance

$$g(bL) = \frac{1}{1 - T(L)^{-b}} = \frac{1}{1 - (1 + g^{-1})^b}. \tag{4}$$

In the last equality, we have inverted Eq. (3) to replace T. We can now calculate the β-function that characterizes the response of g to changes in system size L.

$$\beta = \frac{d \ln g}{d \ln L} = (d-1) - (1+g) \ln\left(1 + g^{-1}\right). \tag{5}$$

For $g \ll 1$, β is dominated by the logarithmic term and simplifies to $\ln(g)$. For large g, it asymptotically approaches the value $d - 2$. A plot of β is shown in Fig. 2.

In one or two dimensions, the β-function is always negative and, under scaling of the system, the conductance will always decrease, i.e. flow to the stable fixed point at $g = 0$. Hence, the system will be a perfect insulator in the thermodynamic limit. We conclude that for $d = 1, 2$ all states in disordered systems are localized.

In three dimensions, however, there is an unstable fixed point at a critical conductance defined by $\beta(g_c) = 0$. Consequently, g_c marks a metal-insulator phase transition (MIT). From Renormalization Group theory [7], we obtain the critical exponent of this transition with

$$\nu = \left(g_c \beta'(g_c)\right)^{-1} = 1.68, \tag{6}$$

so that the localization length behaves as

$$\xi \propto (W - W_c)^{-\nu} \tag{7}$$

in the vicinity of the critical disorder with $W < W_c$ [6, 8, 9].

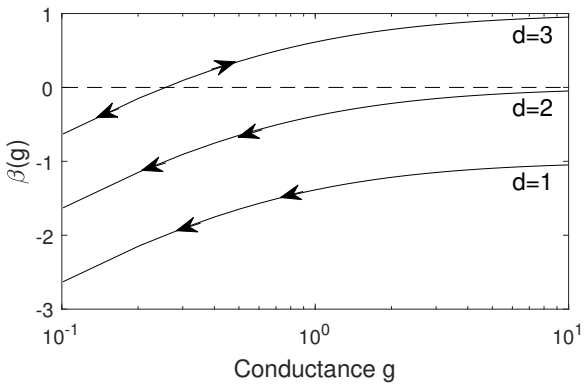

FIG. 2. Scaling function β for 1-3 dimensions. For $d < 3$ the conductance always flows to the stable fixed point at $g = 0$, so that the system will be an insulator in the thermodynamic limit. Only for $d = 3$ is there is an unstable fixed point when $\beta(g_c) = 0$. Here, g_c marks a metal insulator phase transition.

IV. NUMERICAL ANALYSIS OF THE ANDERSON MODEL IN 3D

In Anderson's tight-binding Hamiltonian (1), the strength of disorder is measured by the width W of the on-site energy probability distribution. Following Eq. (7), we expect that, once W surpasses a critical value W_c, electronic eigenfuntions localize in 3D which leads to a MIT. Analytical estimation of the critical disorder, however, is problematic. For a uniform box distribution over $[-W/2, W/2]$, numerical analysis of the 3D Anderson Hamiltonian shows that $W_c \approx 16.5$ [10]. Since W_c is not small compared to the relevant energy scale given by the bandwidth of delocalized electrons in a perfectly ordered 3D crystal ($-6 \leq E \leq 6$), perturbative approaches to determine W_c fail. Nonetheless, it is straightforward to demonstrate the disorder-induced Anderson transition in 3D numerically.

A. Eigenstates

In order to simulate the Anderson transition in three dimensions, we diagonalize the Anderson Hamiltonian (1) for a single particle whose eigenstates $|\psi\rangle = \sum_{\boldsymbol{r}} \psi(\boldsymbol{r}) c^\dagger_{\boldsymbol{r}} |0\rangle$ are defined on a cubic lattice given by the set of vectors $\boldsymbol{r} = n_x \boldsymbol{e}_x + n_y \boldsymbol{e}_y + n_z \boldsymbol{e}_z$, with integers $1 \leq n_x, n_y, n_z \leq N$. In this case, the resulting Schroedinger equation to be solved reads

$$W \epsilon_{\boldsymbol{r}} \psi(\boldsymbol{r}) + \sum_{\alpha = x,y,z} \psi(\boldsymbol{r} + \boldsymbol{e}_\alpha) + \psi(\boldsymbol{r} - \boldsymbol{e}_\alpha) = E \psi(\boldsymbol{r}), \tag{8}$$

with disorder strength W and uniformly distributed random on-site energies, $\epsilon_{\boldsymbol{r}} \in [-1/2, +1/2]$.

Applying periodic boundary conditions along all spatial directions, $\psi(\boldsymbol{r} + N\boldsymbol{e}_\alpha) = \psi(\boldsymbol{r})$, Fig. 3 shows electronic eigenstates near the band center $E \approx 0$ for three

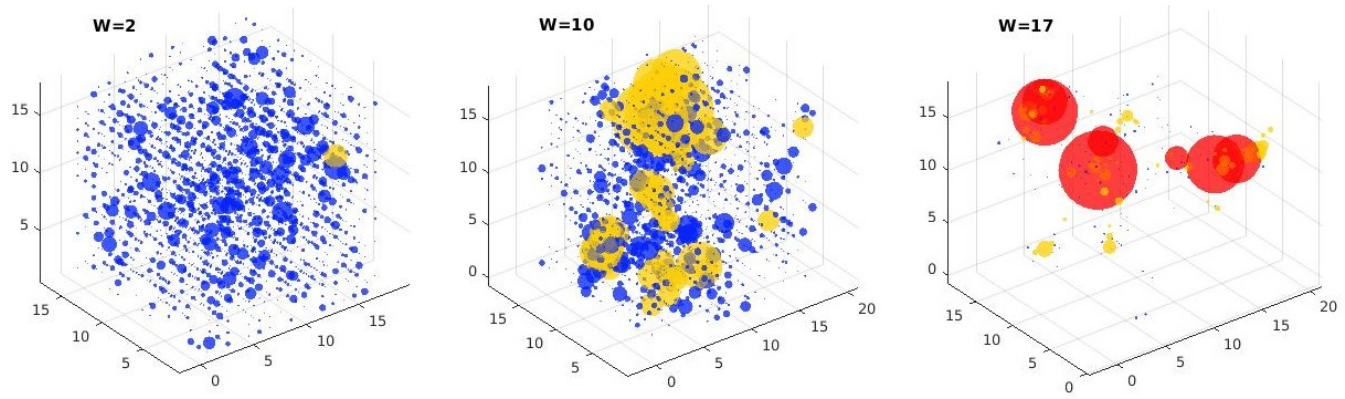

FIG. 3. Anderson localization in 3D of a single-particle inside a $17\times17\times17$ cube. Plotted are eigenfunctions of the Schroedinger Eq. (8) as a function of disorder $W \in \{2, 10, 17\}$. The size of colored spheres indicates the magnitude of probability density $|\psi(\boldsymbol{r})|^2$ at each grid point. Blue spheres display points where $|\psi(\boldsymbol{r})|^2 \leq 0.003$, yellow spheres show $0.003 < |\psi(\boldsymbol{r})|^2 \leq 0.02$, and red spheres correspond to $0.02 < |\psi(\boldsymbol{r})|^2$. Radii in the localized regime $W = 17$ are plotted six times smaller than in the delocalized regime $W = 2(10)$.

disorder realizations of different strength. For weak disorder $W = 2$, the solution resembles an evenly spread probability distribution. This result is not surprising because in the limit $W = 0$ we expect the eigenstates to be Bloch states, such that $|\psi(\boldsymbol{r})|^2 = 1/N^3$ equally for all lattice sites. As we go to stronger disorder $W = 10$, first signatures of localization become evident. Yet, we observe that the eigenstate still spreads over the whole cube and therefore we still ought to be in the metallic regime. Once we reach sufficiently strong disorder $W = 17$ which is above the critical value, $W_c = 16.5$, the system undergoes a MIT. In this regime, we can clearly make out distinct lattice sites where the probability density $|\psi(\boldsymbol{r})|^2$ differs by at least one order of magnitude.

B. Phase diagram

To give a more general picture of the 3D Anderson transition shown in Fig. 3, one can characterize eigenstates of Eq. (8) by use of the *inverse participation ratio* (IPR),

$$I = \sum_{\boldsymbol{r}} |\psi(\boldsymbol{r})|^4. \tag{9}$$

For delocalized states spread uniformly over all lattice sites, the IPR is on the order of $I \sim 1/N^3$. Conversely, localized states are expected to occupy only a few sites and to have an exponentially small probability amplitude elsewhere. The IPR projects out those lattice sites with large probability amplitude and, consequently, yields $I \gg 1/N^3$ for localized states. In Fig. (4), we choose a cubic lattice with $N^3 = 20^3 = 8000$ sites and compute I as a function of disorder W and band energy E. Since the form of eigenstates fed into Eq. (9) depends on the particular disorder realization, we average the IPR over 100 random realizations for a fixed

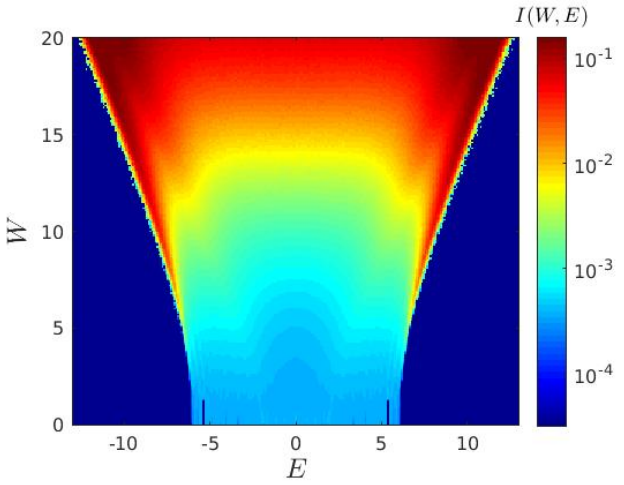

FIG. 4. Metal-insulator transition of the 3D Anderson model. The color map represents the localization strength of electronic eigenstates depending on energy E and disorder W as given by the inverse participation ratio I, cf. Eq. (9). Red indicates stronly localized states, whereas light blue shows completely delocalized states. Energy regions containing no eigenstates are colored dark blue. Disorder varies from $W = 0$ to $W = 20$ with spacing $\Delta W = 0.1$.

strength W. Eigenstate energies are grouped into intervals of width $\Delta E = 0.1$.

Figure 4 confirms that, for weakly disordered systems, eigenstates across the whole band are delocalized with $I \sim 1/8000 \sim 10^{-4}$. As we approach the critical disorder parameter $W_c = 16.5$ [10], I increases by three orders of magnitude which demonstrates the expected transition from the metallic to the insulating regime. Furthermore, the numerical data shows that localization emerges in the energy band edges already below the critical disorder strength, $W < W_c$. In the context of Anderson local-

ization, the threshold $|E| < E_c$ that denotes a MIT for a fixed strength of disorder is commonly referred to as *mobility edge*. A 3D system of noninteracting electrons whose Fermi energy is smaller than the mobility edge, $E_F < E_c$, behaves as an insulator.

V. EXPERIMENTAL EVIDENCE

Early efforts to confirm the existence of localized states focused on conductivity measurements around the MIT of disordered materials. More recent work around 1990s has experimentally demonstrated Anderson localization in a variety of classical and quantum materials, affecting light, acoustic, and matter waves [3]. Here, we will focus on experimental evidence of Anderson localization in matter waves of 1D Bose-Einstein condensates (BEC).

A. Experimental Setup

The direct observation of Anderson localization is in matter waves of 1D rubidium-87 BEC [11]. The BEC is first created in a magneto-optical trap, which employs Doppler cooling on atoms inside a magnetic trap. Evaporative cooling, in which higher energy atoms are "kicked-out" of the magnetic trap using a RF signal, is used to lower the temperature to $\sim 1\mu$K [12]. The BEC is then confined to the transverse z-direction the an optical trap. A weak magnetic trap is used to confine the BEC in the longitudinal direction (Fig. 5).

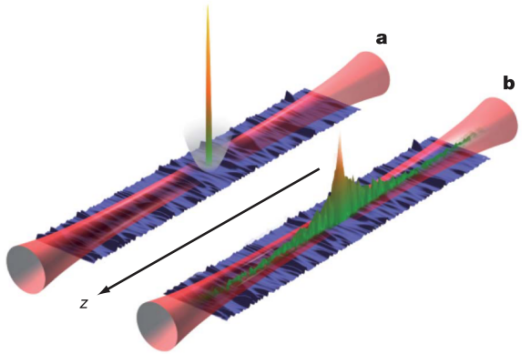

FIG. 5. Experimental setup of [2]. (a) A transverse optical trap is used to confine the BEC to the x and y-direction. A shallow longitudinal magnetic trap is used to hold the BEC before release. (b) After release, the BEC is allowed to evolve in the speckle potential, and the atomic density is measured.

In order to observe Anderson localization, a disorder potential is generated using 1D speckle created by a laser beam sent through a diffusing plate. The longitudinal magnetic trap is then released, and the BEC is allowed to evolve in the potential. The atomic density is observed through absorption and fluorescence imaging [11].

B. 1D Localization Length in Speckle Potential

The localization length of the 1D system in a speckle potential can be theoretically predicted. First, consider a trapped 1D Bose-Einstein condensate (BEC) in a harmonic potential $V_{ho} = m\omega^2 z^2/2$. At some large time after release $t \gg 1/\omega$, atom-atom interactions are negligible, and the wavefunction becomes [13]

$$\psi(z,t) = \frac{\psi(z/b(t),0)}{\sqrt{b(t)}} \exp\left(\frac{imz^2\dot{b}(t)}{2\hbar b(t)}\right), \tag{10}$$

where $b(t)$ is a scaling parameter, with $b(0) = 1$, and $b(t) \approx \sqrt{2}\omega t$ for large times.

Now let the speckle potential be turned on after release. The wavefunction is a superposition of plane-waves

$$\psi(z,t) = \int \frac{dk}{\sqrt{2\pi}} \hat{\psi}(k,t) \exp(ikz). \tag{11}$$

According to Anderson [1], the exponential components of Eq. (11) will become localized functions $\phi_k(z)$ due to the speckle potential. The atomic density of the system would then be

$$n_0(z) = \langle|\psi(z)|^2\rangle = \int_{-k_{max}}^{k_{max}} dk \mathfrak{D}(k) \langle|\phi_k(z)|^2\rangle, \tag{12}$$

where $\mathfrak{D}(k) = |\hat{\psi}(k)|^2$ is the momentum distribution of the system, which is constant for long times $t \gg 1/\omega$, as seen in the Fourier transform of Eq. (10). These localized functions can be obtained using diagrammatic perturbation theory, assuming a weak speckle potential ($V_R\sigma_R \ll \frac{\hbar^2 k}{m}\sqrt{k\sigma_R}$), and distances far from the localized state ($|z| \gg \xi$), we have [14]

$$\langle|\phi_k(z)|^2\rangle \propto e^{-2|z|/\xi}, \tag{13}$$

$$\xi \approx \frac{2\hbar^4 k^2}{\pi m^2 V_R^2 \sigma_R (1-k\sigma_R)\Theta(1-k\sigma_R)}. \tag{14}$$

where V_R and σ_R are the potential amplitude and correlation length of the speckle, respectively, Θ is the Heaviside function, and $\xi(k)$ is a length scale defined as the localization length. See that $\xi \propto V_R^{-2}$, as expected in the transfer-matrix calculation (cf. Fig. 1). Since ξ is an increasing function of k, the asymptotic behaviour of the localized function at large $|z|$ is dominated by the largest k values. Thus we expect localized states to fall exponentially at the tails

$$n_0(z) \propto \exp(-|z|/\xi(k_{max})). \tag{15}$$

C. 1D Anderson Localization of BEC

Prior attempts of this experiment have demonstrated reduced transport in the BEC, however this was attributed to scattering and inter-atomic interactions [15,

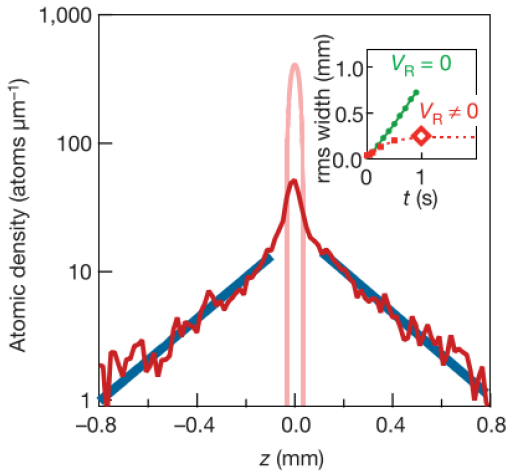

FIG. 6. The atomic density profile of the BEC at $t = 1$s [11]. The pink profile shows the condensate trapped at $t = 0$s. The blue lines are the exponential fits to the tails. The inset shows the rms width of the profile as a function of time for $V_R = 0$ and $V_R \neq 0$, demonstrating the localization of the state. The red diamond corresponds to the point at which the profile is taken.

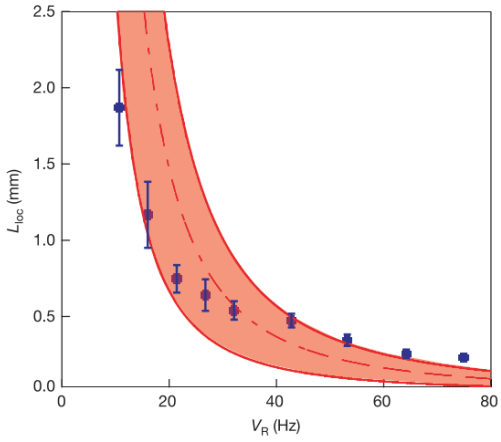

FIG. 7. Localization length as a function of disorder potential from the experimental fit compared with theoretical expression [11]. The blue points are the fit results; the error bars represent 95% confidence interval for fit values. The dash-dot line represents the theoretical result in Eq. (14), with the shaded area being uncertainty evaluations of k_{max}.

16]. To avoid this, the speckle amplitude is small to ensure localization is not due to scattering off of the potential, and the initial atomic density was reduced to minimize atom-atom interactions [11]. At these limits, the above Eqs. (13) and (14) are valid.

The atomic densities are measured at different times as the matter wave evolves through the potential, shown in Fig. 6. The tails were found to be best modelled with an exponential fit of the form of Eq. (15).

If the localized state is a result of Anderson localization, the localization lengths from the fits should agree with the values of $\xi(k_{max})$ of Eq. (14), where k_{max} is obtained by allowing the BEC to expand in the wave guide with $V_R = 0$. Indeed the results are in agreement, demonstrating that 1D Anderson localization is possible, and measurable (Fig. 7).

D. Experimental Evidence in Higher Dimensions

Experiments looking at higher dimensions of Anderson localization have been done, and compared with theoretical results of scaling theory. For example, in 2D, Anderson localization of light waves has been observed, with specially engineered optical fibres acting as "photonic lattices". Materials with adjustable indices of refraction are used to vary the level of disorder in the system.

For localization in 3D, experiments have mainly focused on electronic transport, the original field from which Anderson derived his theory. While MITs are observed in conductive materials, the critical exponent of the phase transition was found to be close to unity, incompatible with the predicted value of $\nu = 1.68$ in Eq. (6) [17]. Electron-electron interactions were hypothesized to be the cause of the disparity.

There have additionally been experiments involving other types of waves, i.e. electromagnetic or ultrasonic, that demonstrated transmission levels consistent with those predicted by scaling theory.

VI. CONCLUSION

In the present work, we have explored the effects of disorder in a tight binding model. In one dimension, an arbitrarily small random on-site energy localizes all eigenstates, so that the wavefunctions are confined to a specific region of the lattice and the system is characterized by an absence of diffusion in the thermodynamic limit. Using scaling arguments, we have extended this result to two dimensions. Only for $d \geq 3$, there is a second-order metal insulator phase transition. We have numerically calculated a phase diagram for this transition by exact diagonalization of the 3D-Hamiltonian of a cubic lattice with 20^3 sites.

Finally, we have reviewed recent experimental evidence of localization of a one dimensional Bose-Einstein condensate in an optical trap. Here, direct imaging of the wavefunction reveals localization in good agreement to numerical and analytical predictions.

VII. ACKNOWLEDGEMENTS

We would like to thank Mona Berciu for the assignment of this project. Computations were facilitated by high-performance computing resources of the UBC Stewart Blusson Quantum Matter Institute.

[1] P. W. Anderson, Physical Review **109**, 1492 (1958).
[2] A. Aspect and M. Inguscio, Phys. Today **62**, 30 (2009).
[3] A. Lagendijk, B. van Tiggelen, and D. S. Wiersma, Physics Today **62**, 24 (2009).
[4] H. Furstenberg and H. Kesten, The Annals of Mathematical Statistics **31**, 457 (1960).
[5] K. Ishii, Progress of Theoretical Physics Supplement **53**, 77 (1973).
[6] E. Abrahams, P. W. Anderson, D. C. Licciardello, and T. V. Ramakrishnan, Physical Review Letters **42**, 673 (1979).
[7] M. Kardar, *Statistical physics of fields*, 6th ed. (Cambridge University Press, Cambridge [etc.], 2013).
[8] R. Beig, G. Englert, U. Frisch, P. Hänggi, K. Hepp, W. Hillebrandt, D. Imboden, R. L. Jaffe, R. Lipowsky, H. v. Löhneysen, I. Ojima, D. Sornette, S. Theisen, W. Weise, J. Wess, J. Zittartz, T. Brandes, and S. Kettemann, *Anderson Localization and Its Ramifications*, Vol. 630 (Springer Berlin Heidelberg, Berlin, Heidelberg, 2003).
[9] Cord A. Mueller, Dominique Delande, "Disorder and interference: localization phenomena," (2016).
[10] T. Brandes and S. Kettemann, *Anderson Localization and Its Ramifications: Disorder, Phase Coherence, and Electron Correlations*, Lecture Notes in Physics (Springer Berlin Heidelberg, 2003).
[11] J. Billy, V. Josse, Z. Zuo, A. Bernard, B. Hambrecht, P. Lugan, D. Clément, L. Sanchez-Palencia, P. Bouyer, and A. Aspect, Nature **453**, 891 (2008), arXiv:0804.1621.
[12] W. Guerin, J. F. Riou, J. P. Gaebler, V. Josse, P. Bouyer, and A. Aspect, Physical Review Letters **97** (2006), 10.1103/PhysRevLett.97.200402, arXiv:0607438 [cond-mat].
[13] Y. Kagan, E. L. Surkov, and G. V. Shlyapnikov, Physical Review A **54**, R1753 (1996), arXiv:9606001 [atom-ph].
[14] L. Sanchez-Palencia, D. Clément, P. Lugan, P. Bouyer, G. V. Shlyapnikov, and A. Aspect, Physical Review Letters **98** (2007), 10.1103/PhysRevLett.98.210401, arXiv:0612670 [cond-mat].
[15] D. Clément, A. F. Varon, M. Hugbart, J. A. Retter, P. Bouyer, L. Sanchez-Palencia, D. M. Gangardt, G. V. Shlyapnikov, and A. Aspect, Physical Review Letters **95**, 170409 (2005).
[16] C. Fort, L. Fallani, V. Guarrera, J. Lye, M. Modugno, D. Wiersma, and M. Inguscio, Physical review letters **95**, 170410 (2005).
[17] S. Katsumoto, F. Komori, N. Sano, and S.-i. Kobayashi, Journal of the Physical Society of Japan **56**, 2259 (1987).
[18] R. Nandkishore and D. A. Huse, Annual Review of Condensed Matter Physics **6**, 15 (2015).
[19] D. A. Abanin and Z. Papić, Annalen der Physik **529**, 1700169 (2017).
[20] J. M. Deutsch, Physical Review A **43**, 2046 (1991).
[21] M. Srednicki, Physical Review E **50**, 888 (1994).
[22] M. Srednicki, "Does quantum chaos explain quantum statistical mechanics?" .
[23] R. Islam, R. Ma, P. M. Preiss, M. E. Tai, A. Lukin, M. Rispoli, and M. Greiner, Nature **528**, 77 (2015).
[24] A. M. Kaufman, M. E. Tai, A. Lukin, M. Rispoli, R. Schittko, P. M. Preiss, and M. Greiner, Science (New York, N.Y.) **353**, 794 (2016).

Appendix A: Electron-Electron Interactions

In the previous part, we have neglected electron-electron interactions. This approximation is only reasonable for systems that behave ideally, such as BEC. For an improved theoretical description, we will add an on-site repulsion term to our Anderson Hamiltonian (1) and obtain the Bose-Hubbard Hamiltonian with random on-site potential

$$\hat{H} = W \sum_n \epsilon_n \hat{c}_n^\dagger \hat{c}_n + t \sum_{<n,m>} \left(\hat{c}_n^\dagger \hat{c}_m + \text{h.c.} \right) + \frac{U}{2} \sum_n \hat{n}_n (\hat{n}_n - 1). \quad \text{(A1)}$$

The study of localization phenomena of interacting systems defines the area of many-body localization (MBL). This is an area of active research with many questions to be answered [18, 19]. In the following, we will discuss the single most notable implication of MBL - the failure of localized systems to thermalize.

1. Eigenstate Thermalization Hypothesis (ETH)

We consider an isolated quantum system that we partition in parts A and B. Originally, this system is prepared in state

$$|\psi\rangle = \sum_{ab} c_{ab} |a\rangle_A \otimes |b\rangle_B .$$

We can readily write down the density matrix for subsystem A:

$$\rho_A = tr_B \left(|\Psi\rangle \langle\Psi| \right) = \sum_b \begin{pmatrix} |c_{0b}| & c_{0b}^* c_{1b} & \dots \\ \vdots & \ddots & \\ c_{Nb} c^* c_{0b} & & |c_{Nb}| \end{pmatrix}. \quad \text{(A2)}$$

The Eigenstate Thermalization Hypothesis now states [20–22], that if

1. the diagonal terms of ρ_A are a smooth function of energy E of state $|\Psi\rangle$

2. the off-diagonal terms decohere (i.e. interfere destructively since they are the sum of many oscillating terms of different frequencies)

- then, the reduced density matrix will be equal to a statistical density matrix (i.e. canonical) after some equilibration time. We can write this as

$$\rho_A = \rho_A^{th} = \exp\left(-\beta \hat{H}_A \right). \quad \text{(A3)}$$

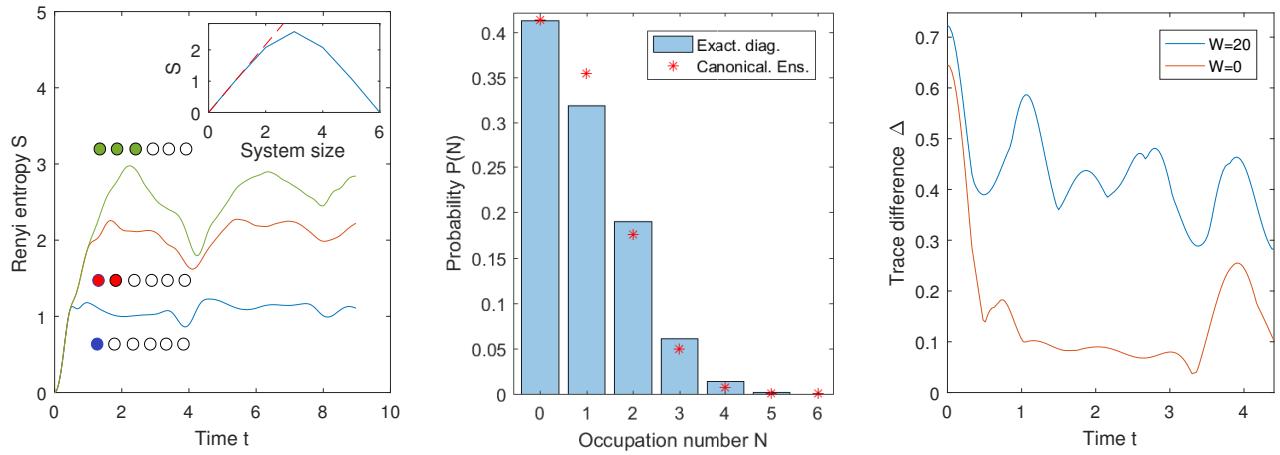

FIG. 8. (left) Time evolution of entanglement entropy for subsystems of size 1-3. The initial state $|\Psi_0\rangle$ is not entangled. Renyi entropy shows an initial increase and then fluctuates around a saturated value. The inset plots the average saturated value over system size. For small system sizes, the entropy follows a volume law (red dashed line). (middle) On-site statistics for a single site at $t = 10$. Blue bars display the probability $P(N)$ of occupation number N. Red marks are predictions of a canonical ensemble. The two values show reasonable agreement, indicating that the system has thermalized. (right) Trace difference $\Delta = tr\left(|\rho_A - \rho_A^{th}|\right)$ for disorder $W = 0, 20$. For $W = 0$, Δ decreases and then fluctuates at low values around ~ 0.1, while for $W = 20$ the saturation value is ~ 0.4. Thus, for high disorder, the quantum mechanical description differs substantially from the canonical prediction, indicating that the system is many-body localized.

The effective temperature β in the canonical description is obtained by requiring that the expectation values of the energy are the same:

$$\langle\Psi(0)|\,\hat{H}\,|\Psi(0)\rangle = tr(\rho^{th}\hat{H}).$$

Simply put, this means: A small isolated quantum system may act as its own bath and thermalize.

This result may seem astonishing to the reader, and we will not give further justification of this hypothesis and refer to references [18, 21] for detailed discussion. We note however, that this hypothesis - if true - is of great benefit. The numerical calculation of density matrices for isolated quantum systems is only possible for fairly small system sizes while the statistical treatment does not require much effort for arbitrary dimension of the Hilbert-space.

To test the ETH, we simulate a bosonic chain of six sites at half filling with the Hamiltonian (A1). For now, all $\epsilon_n = 0$. We time involve the initial state $|\Psi(t = 0)\rangle = |111111\rangle$. This, of course, is not an eigenstate and has an energy far from the ground level. All results are obtained by exact diagonalization of the 462-dimensional Hilbert space.

The ETH requires off-diagonal terms in Eq. (A2) to decohere. This process will likely cause entanglement between the subsystems, since $\rho = \rho^2$ only holds for a diagonal matrix with $\rho_{n,n} = \delta_{n,k}$. Thus, we expect time evolution of entanglement to give valuable insight into the thermalization process. We define the Renyi entropy $S = -tr\left(\rho^2\right)$ as a measure of entanglement.

The left graph of Fig. A3 shows the Renyi entropy S as a function of time for three different subsystems consisting of 1 (blue), 2 (red), and 3 (green) sites. After an initial growth, the entanglement entropy fluctuates around a saturated value. Fluctuations are higher for larger subsystems.

As a consequence of the ETH, the Renyi entropy should be equal to a statistical entropy. Then, since entropy is an extensive quantity, S should obey a volume law. To prove this requirement, we have plotted the saturated value of the entropy as a function of system size in the inset of Fig. A3. As expected, the entropy S follows a volume law (red dashed line) for small system sizes and then bends back due to symmetry.

Another way to observe the effects of thermalization, is to compare the on-site statistics predicted by exact diagonalization and the canonical density matrix. Blue bars in the middle panel of Fig. A3 show probabilities $P(N)$ of occupation number N for a one-site subsystem at $t = 10$. Clearly, these values closely resemble the canonical predictions marked by red points.

Last, we directly measure the differences of density matrices ρ_A and ρ_A^{th} by computing the trace difference $\Delta = tr\left(|\rho_A - \rho_A^{th}|\right)$. The red curve in the right panel of Fig. A3 shows Δ as a function of time. The initially high trace difference decreases to low values around ~ 0.1. This is clear evidence of the validity of the ETH in the Bose-Hubbard model.

At this point, we would like to note, that recent advances in experimental techniques allow for accurate experimental measurements of all quantities in Fig. A3. The reader may be referred to references [23, 24].

2. Many-Body Localization (MBL)

Let us now introduce some disorder. We diagonalize the Hubbard-Hamiltonian for a disorder parameter $W = 20$ and plot the trace difference Δ as the blue curve in the right panelof Fig. A3. The high values of ~ 0.4 compared to the case $W = 0$ suggest that disorder has in fact prevented the system from thermalization. This is a strong indicator of MBL. Note that this analysis is only meant to be of qualitative nature. For a more rigorous argument, the trace difference Δ needs to be averaged over many different realizations of random on-site energy.